Chapter 6

Vibration Control of an Inflated Torus

6.1 Introduction

Our objective in this chapter is to design a controller in order to suppress the vibration of the inflated torus using piezoelectric actuators and sensors. In Chapter 5, we designed actuators and sensors optimally and calculated the natural frequencies and mode shapes of the inflated torus including the passive effects of the piezoelectric patches. These results will be used here in obtaining the mathematical models of the plant (inflated torus) and actuator/sensor interactions. This will provide the state-space model of the system. The main remaining task will then be to find a suitable controller. Once successfully designed, the controller should be able to find the actuator voltages based on the sensor outputs so that the vibration of the torus reduces over time.

Several assumptions have been made in calculating the vibration characteristics of the inflated torus and actuator/sensor models. The errors due to these mathematical simplifications lead to the so-called model uncertainty. In addition, the operating condition of the inflatable antenna varies and it may be subjected to unknown disturbances. Given these facts, it is important to consider a robust controller, which can function properly even in the presence of model uncertainties and disturbances. To this end, we use a sliding mode controller and sliding mode observer. The basics of the sliding mode controller and observer are presented in the next sections. Thereafter, these techniques are applied to the torus problem considering the first nine modes, five actuators, and five sensors.

Due to practical limitation, we generally consider only a few lower modes of a distributed structure for the control problem. Actuator forces, meant to reduce the vibration in these modes, will also influence the other modes of the structure, producing undesirable vibration due to the uncontrolled modes. This phenomenon is known as control spillover. Similarly, the sensor will sense the deflection not only from the controlled modes but from the other modes as well, giving rise to the so-called observation spillover. While the control spillover effect can degrade the performance of a controller, it cannot destabilize the system. On the other hand, the observation spillover can destabilize the system apart from degrading the performance of the controller. The control and observation spillover effect will be demonstrated and special attention will be paid to reduce the observation spillover effect.

Finally, we concentrate upon the effects of external disturbance and parametric uncertainty. Out of the several sources of parametric uncertainties, we consider the one arising from the changes in internal pressure of the torus. As the inflatable satellite encircles the earth, it is subjected to varied sunlight and hence variations in temperatures and internal pressures. This causes changes in the dynamic characteristics of the torus. Besides, these satellites are often subjected to external disturbances. A controller should be able to reduce the vibration even in these circumstances. This is attempted in the last section of this chapter, where we use numerical simulations to show the performance of the sliding mode controller and observer in the presence of disturbances and uncertainty.

6.2 Control Strategy

We saw in Chapter 4 that an inflated torus has several close frequencies and quite complicated mode shapes. We also saw that the natural frequencies and mode shapes are quite sensitive to changes in different structural parameters and internal pressure. In solving the free vibration problem, we made several assumptions in order to simplify the mathematical model. This includes, to name a few, constant pressure during vibration, circular cross-section of the inflated torus after the static deformation, ignoring the nonlinear terms in the bending strain-displacement relations, and ignoring the nonlinear dynamics and material nonlinearity due to high initial deflection. Also, the solutions are not exact but rather obtained using an approximate method. While we assumed free boundary conditions, in reality the inflated torus is attached with an inflatable mirror. Similarly, in Chapter 5, we saw that the modal forces and modal sensing constants are fairly sensitive to the patch sizes and locations. Again assumptions were made, such as perfect bonding between the structure and the patches, zero bonding thickness, linear operation region, and so on. Inaccuracies in the model also come from the fact that the inflatable satellite operates in a changing environment, which tends to change the dynamic characteristics of the torus. These observations suggest that the state-space model of the system will be somewhat different from the actual case, giving rise to the so-called model uncertainty. Moreover, the satellites are often subjected to unknown disturbances coming from several sources, such as meteoroid impacts, thermal shock, satellite repositioning, and imbalance of the onboard rotating gyroscope. The on-board controller should be able to achieve vibration reduction in the presence of these uncertainties and disturbances. This leads to the requirement of a robust controller. Moreover, the observer, which estimates the states from the output measurement given by the sensors, also needs to perform under these adverse conditions. This requires that the observer should also have the robustness properties against the model uncertainty and disturbances.

In this study, we use sliding mode controller and observer. They can be proved to be robust against a special class of uncertainty, called matched uncertainty. The control system

is characterized by the existence of a sliding motion, which results as the controller compels the system to follow a certain manifold in the state-space, known as the sliding surface. In order to maintain the sliding motion, the controller produces discontinuous (or, nearly discontinuous) actuator forces. Essentially, the uncertainties are compensated by the nonlinear part of the controller, which is responsible for the sliding motion. A similar strategy is applied in designing a sliding mode observer. Details of the design process are described next.

6.3 Sliding Mode Control

Sliding mode control methodology is a subclass of Variable Structure Control, where the control law is accompanied by a set of decision rules. Several papers and books have been written on the subject of sliding mode control (Utkin, 1978; DeCarlo et al., 1988; Yurkovitch, et al., 1988; Kao and Sinha, 1992; Choi, Cheong, and Kim, 1997; Matheu, 1997; Edward and Spurgeon, 1998; Tang, Wang, and Philen, 1999). The sliding mode design approach consists of two steps. In the first step, a sliding surface is designed so that the controller satisfies some time- or frequency-domain characteristics. The second step is to design a control law such that the system remains on (or close to) the sliding surface. We summarize here briefly both the steps. A detailed discussion on this topic can be found in the references, such as Edward and Spurgeon (1998). The state-space model, given by Eqs. (3.41), can be modified slightly in order to incorporate the uncertainty in the following form:

$$\dot{\boldsymbol{x}} = \boldsymbol{A}\,\boldsymbol{x} + \boldsymbol{B}\,\boldsymbol{u} + \boldsymbol{f}(t, \boldsymbol{x}, \boldsymbol{u}), \tag{6.1}$$

where $\boldsymbol{f}(t, \boldsymbol{x}, \boldsymbol{u})$ is the unknown function representing the model uncertainty or disturbances, $\boldsymbol{x}$ is the state vector of length n, and $\boldsymbol{u}$ is the vector of actuator voltages of length m. The system $(\boldsymbol{A}, \boldsymbol{B})$ is assumed to be controllable. We assume that $\boldsymbol{f}(t, \boldsymbol{x}, \boldsymbol{u})$ is the so-called matched uncertainty. This means that $\boldsymbol{f}(t, \boldsymbol{x}, \boldsymbol{u})$ can be written in terms of the input matrix $\boldsymbol{B}$ and another disturbance function $\xi(t, \boldsymbol{x}, \boldsymbol{u})$ as

$$\boldsymbol{f}(t,\boldsymbol{x},\boldsymbol{u}) = \boldsymbol{B}\xi(t,\boldsymbol{x},\boldsymbol{u}). \tag{6.2}$$

Now, we define a switching function, $\boldsymbol{s}(t)$, as

$$\boldsymbol{s}(t) = \boldsymbol{S}\,\boldsymbol{x}(t), \tag{6.3}$$

where $\boldsymbol{S}$ is a matrix of size $m \times n$ defining the hyperplane on which the sliding occurs when the switching function becomes zero. This implies that the sliding surface can be regarded as the solution space of a set of homogeneous linear equations, given by

$$\boldsymbol{s}(t) = \boldsymbol{S}\,\boldsymbol{x}(t) = 0. \tag{6.4}$$

The role of the control system is to drive the system towards this sliding surface and keep on or close to the sliding surface. The resulting motion is called sliding motion.

In order to see the effect of control input on uncertainty and sliding motion, it is convenient to write Eq. (6.1) in a regular form (Utkin, 1971). Let $\boldsymbol{T}$ be a linear transformation of dimension $n \times n$ such that

$$\boldsymbol{T}^T\,\boldsymbol{B} = \begin{bmatrix} \boldsymbol{0} \\ \boldsymbol{B_2} \end{bmatrix}, \tag{6.5}$$

where $\boldsymbol{B_2}$ is an square matrix of full rank and size $m \times m$ and the transformation matrix $\boldsymbol{T}$ can be obtained using Gaussian elimination or QR decomposition (Edward and Spurgeon, 1998). Now, we define the following state transformation relating the states $\boldsymbol{x}(t)$ with some new states $\boldsymbol{y}(t)$:

$$\boldsymbol{x}(t) = \boldsymbol{T}\,\boldsymbol{y}(t). \tag{6.6}$$

Using Eq. (6.5), we can rewrite Eq. (6.1) in terms of $\boldsymbol{y}(t)$ as

$$\dot{\boldsymbol{y}} = \overline{\boldsymbol{A}}\,\boldsymbol{y} + \overline{\boldsymbol{B}}\,\boldsymbol{u} + \bar{\boldsymbol{f}}(t, \boldsymbol{y}, \boldsymbol{u}), \tag{6.7}$$

where $\overline{\boldsymbol{A}} = \boldsymbol{T}^T \boldsymbol{A}\boldsymbol{T}$, $\overline{\boldsymbol{B}} = \boldsymbol{T}^T \boldsymbol{B}$, and $\bar{\boldsymbol{f}} = \boldsymbol{T}^T \boldsymbol{f}$. In deriving Eq. (6.6), we used the fact that $\boldsymbol{T}$ is a unitary matrix, i.e.,

$$\boldsymbol{T}^{-1} = \boldsymbol{T}^T. \tag{6.8}$$

The switching function, $\boldsymbol{s}(t)$, can also be written in terms $\boldsymbol{y}(t)$ as

$$\boldsymbol{s}(t) = \overline{\boldsymbol{S}}\,\boldsymbol{y}(t), \tag{6.9}$$

where the new hyperplane of the sliding motion, $\overline{\boldsymbol{S}}$, can be obtained from $\boldsymbol{S}$ using the relation

$$\overline{\boldsymbol{S}} = \boldsymbol{S}\boldsymbol{T}. \tag{6.10}$$

Now, the state vector $\boldsymbol{y}(t)$ can be partitioned into two vector parts $\boldsymbol{y_1}(t)$ and $\boldsymbol{y_2}(t)$ of lengths $n-m$ and m, respectively, and Eq. (6.7) can be written as

$$\dot{\boldsymbol{y}}_1(t) = \boldsymbol{A_{11}}\,\boldsymbol{y_1}(t) + \boldsymbol{A_{12}}\,\boldsymbol{y_2}(t), \quad \dot{\boldsymbol{y}}_2(t) = \boldsymbol{A_{21}}\,\boldsymbol{y_1}(t) + \boldsymbol{A_{22}}\,\boldsymbol{y_2}(t) + \boldsymbol{B_2}\,\{\boldsymbol{u}(t) + \boldsymbol{\xi}(t, \boldsymbol{x}, \boldsymbol{u})\}, \tag{6.11}$$

where $\boldsymbol{A_{11}}$, $\boldsymbol{A_{12}}$, $\boldsymbol{A_{21}}$, and $\boldsymbol{A_{22}}$ are the block partitioned matrices of $\overline{\boldsymbol{A}}$. The above representation of the state-space model is called the regular form. Similarly, Eq. (6.9) can be written as

$$\boldsymbol{s}(t) = \boldsymbol{S_1}\,\boldsymbol{y_1}(t) + \boldsymbol{S_2}\,\boldsymbol{y_2}(t). \tag{6.12}$$

By eliminating $\boldsymbol{y_2}(t)$ from Eq. (6.12), one can write Eqs. (6.11) as

$$\dot{\boldsymbol{y}}_{\boldsymbol{1}}(t) = \overline{\boldsymbol{A}}_{\boldsymbol{11}}\, \boldsymbol{y}_{\boldsymbol{1}}(t) + \boldsymbol{A}_{\boldsymbol{12}}\, \boldsymbol{S}_{\boldsymbol{2}}^{-1}\, \boldsymbol{s}(t)\,,$$

$$\dot{\boldsymbol{s}}(t) = \boldsymbol{S}_{\boldsymbol{2}} \overline{\boldsymbol{A}}_{\boldsymbol{21}}\, \boldsymbol{y}_{\boldsymbol{1}}(t) + \boldsymbol{S}_{\boldsymbol{2}} \overline{\boldsymbol{A}}_{\boldsymbol{22}}\, \boldsymbol{S}_{\boldsymbol{2}}^{-1} \boldsymbol{s}(t) + \boldsymbol{S}_{\boldsymbol{2}} \boldsymbol{B}_{\boldsymbol{2}} \{\boldsymbol{u}(t) + \xi(t, \boldsymbol{x}, \boldsymbol{u})\}\,, \tag{6.13}$$

where $\overline{\boldsymbol{A}}_{\boldsymbol{11}} = \boldsymbol{A}_{\boldsymbol{11}} - \boldsymbol{A}_{\boldsymbol{12}}\boldsymbol{M}$, $\overline{\boldsymbol{A}}_{\boldsymbol{21}} = \boldsymbol{M}\, \overline{\boldsymbol{A}}_{\boldsymbol{11}} + \boldsymbol{A}_{\boldsymbol{21}} - \boldsymbol{A}_{\boldsymbol{22}}\boldsymbol{M}$, $\overline{\boldsymbol{A}}_{\boldsymbol{22}} = \boldsymbol{M}\, \boldsymbol{A}_{\boldsymbol{12}} + \boldsymbol{A}_{\boldsymbol{22}}$, and $\boldsymbol{M} = \boldsymbol{S}_{\boldsymbol{2}}^{-1}\boldsymbol{S}_{\boldsymbol{1}}$. The control input $\boldsymbol{u}(t)$ can be written in two separate groups:

$$\boldsymbol{u}(t) = \boldsymbol{u}_{\boldsymbol{l}}(t) + \boldsymbol{u}_{\boldsymbol{n}}(t)\,, \tag{6.14}$$

where the linear part $\boldsymbol{u}_{\boldsymbol{l}}(t)$ and the nonlinear part $\boldsymbol{u}_{\boldsymbol{n}}(t)$ can be given by

$$\boldsymbol{u}_{\boldsymbol{l}}(t) = (\boldsymbol{S}_{\boldsymbol{2}}\boldsymbol{B}_{\boldsymbol{2}})^{-1} \{-\boldsymbol{S}_{\boldsymbol{2}}\, \overline{\boldsymbol{A}}_{\boldsymbol{21}}\, \boldsymbol{y}_{\boldsymbol{1}}(t) - (\boldsymbol{S}_{\boldsymbol{2}}\, \overline{\boldsymbol{A}}_{\boldsymbol{22}}\, \boldsymbol{S}_{\boldsymbol{2}}^{-1} - \boldsymbol{\Phi})\, \boldsymbol{s}(t)\}\,,$$

$$\boldsymbol{u}_{\boldsymbol{n}}(t) = -\rho_c(t, \boldsymbol{x})(\boldsymbol{S}_{\boldsymbol{2}}\boldsymbol{B}_{\boldsymbol{2}})^{-1} \frac{\boldsymbol{P}_{\boldsymbol{2}}\boldsymbol{s}(t)}{\left\|\boldsymbol{P}_{\boldsymbol{2}}\boldsymbol{s}(t)\right\| + \delta}\,, \tag{6.15}$$

where $\boldsymbol{\Phi}$ is a stable design matrix, δ is a small number to reduce the chattering of actuators, and $\boldsymbol{P}_{\boldsymbol{2}}$ is a symmetric positive definite matrix satisfying the Lyapunov equation

$$\boldsymbol{P}_{\boldsymbol{2}}\, \boldsymbol{\Phi} + \boldsymbol{\Phi}^T\, \boldsymbol{P}_{\boldsymbol{2}} = -\boldsymbol{I}\,. \tag{6.16}$$

The magnitude of ρ_c depends on the degree of uncertainty and should be high enough to counteract it. We use a quadratic minimization technique to design the sliding surface $\overline{\boldsymbol{S}}$. The proof of Lyapunov stability and the design procedure for the sliding surface can be found in Edward and Spurgeon (1998).

6.4 Sliding Mode Observer

The controller described in the above section uses all the state information in order to generate the control signal. In many cases, it is quite difficult or impossible to measure all the states. For example, some states may be abstract quantities rather than being physically measurable. In those cases, in order to use a state-based controller, such as that described above, an observer is needed to estimate the states, given some output data. The reasons, which necessitated the use of a robust controller, also justify implementing a robust observer. Otherwise, the estimated states will not be accurate in the presence of uncertainty, and hence the controller performance will be adversely affected even if the controller is robust. To this end we choose to work with a sliding mode observer. We derive the basic elements of such an observer based upon the work of Utkin (1992). The output equation, relating the sensor voltage to the states of the system (Eq. 6.1), can be written as

$$\boldsymbol{y}(t) = \boldsymbol{C}\,\boldsymbol{x}(t)\,. \tag{6.17}$$

Consider a transformation

$$\boldsymbol{z}(t) = \boldsymbol{T_c}\,\boldsymbol{x}(t)\,, \tag{6.18}$$

where

$$\boldsymbol{T_c} = \begin{bmatrix} \boldsymbol{N_c}^T \\ \boldsymbol{C} \end{bmatrix}. \tag{6.19}$$

The matrix $\boldsymbol{N_c}^T$ is chosen such that its column spans the null space of the output matrix $\boldsymbol{C}$. It follows from this transformation that

$$\boldsymbol{C}\,\boldsymbol{T_c}^{-1} = [\boldsymbol{0},\, \boldsymbol{I}]\,. \tag{6.20}$$

Substituting the transformation from Eq. (6.18) in Eqs. (6.1) and (6.17) gives

$$\dot{\boldsymbol{z}} = \boldsymbol{T_c A T_c^{-1}} \boldsymbol{z}(t) + \boldsymbol{T_c B}\, \boldsymbol{u}(t) + \boldsymbol{T_c}\, \boldsymbol{f}(t, x, u)\,, \tag{6.21}$$

$$\boldsymbol{y}(t) = \boldsymbol{C T_c^{-1}} \boldsymbol{z}(t)\,. \tag{6.22}$$

Simplification of Eq. (6.22) gives

$$\boldsymbol{y}(t) = [\boldsymbol{0}, \boldsymbol{I}]\, \boldsymbol{z}(t) = [\boldsymbol{0}, \boldsymbol{I}] \begin{Bmatrix} \boldsymbol{z_1}(t) \\ \boldsymbol{z_2}(t) \end{Bmatrix} = \boldsymbol{z_2}(t)\,, \tag{6.23}$$

where $\boldsymbol{z_1}(t)$ and $\boldsymbol{z_2}(t)$ are of appropriate dimensions. Using Eq. (6.23), we can write Eqs. (6.21) and (6.22) as

$$\dot{\boldsymbol{z}}_{\boldsymbol{1}} = \boldsymbol{A_{11o}}\, \boldsymbol{z_1} + \boldsymbol{A_{12o}}\, \boldsymbol{y} + \boldsymbol{B_{1o}}\, \boldsymbol{u} + \boldsymbol{f_{1o}}\,,$$

$$\dot{\boldsymbol{y}} = \boldsymbol{A_{21o}}\, \boldsymbol{z_1} + \boldsymbol{A_{22o}}\, \boldsymbol{y} + \boldsymbol{B_{2o}}\, \boldsymbol{u} + \boldsymbol{f_{2o}}\,. \tag{6.24}$$

Based upon the above two equations, we can design an observer of the following form (Utkin, 1992; Edward and Spurgeon, 1998):

$$\dot{\hat{\boldsymbol{z}}}_{\boldsymbol{1}} = \boldsymbol{A_{11o}}\, \hat{\boldsymbol{z}}_{\boldsymbol{1}} + \boldsymbol{A_{12o}}\, \hat{\boldsymbol{y}} + \boldsymbol{B_{1o}}\, \boldsymbol{u} - \boldsymbol{G_1}(\hat{\boldsymbol{y}} - \boldsymbol{y}) + \boldsymbol{L v}\,,$$

$$\dot{\hat{\boldsymbol{y}}} = \boldsymbol{A_{21o}}\, \hat{\boldsymbol{z}}_{\boldsymbol{1}} + \boldsymbol{A_{22o}}\, \hat{\boldsymbol{y}} + \boldsymbol{B_{2o}}\, \boldsymbol{u} - \boldsymbol{G_2}(\hat{\boldsymbol{y}} - \boldsymbol{y}) - \boldsymbol{v}\,, \tag{6.25}$$

where the quantities with hats are the estimated quantities from the observer, $\boldsymbol{v}$ is a nonlinear parameter defined later, and $\boldsymbol{G_1}$, $\boldsymbol{G_2}$ are the gains. Subtracting Eqs. (6.24) from Eqs. (6.25), we get

$$\dot{e}_1 = A_{11o}\, e_1 + A_{12o}\, e_y - f_{1o} - G_1\, e_y + Lv\,,$$

$$\dot{e}_y = A_{21o}\, e_1 + A_{22o}\, e_y - f_{2o} - G_2\, e_y - v\,, \tag{6.26}$$

where the errors $e_1 = \hat{z}_1 - z_1$ and $e_y = \hat{y} - y$. Now use the following substitution in the above equation:

$$\bar{e}_1 = e_1 + L e_y\,. \tag{6.27}$$

After some simplifications, Eq. (6.26) becomes

$$\dot{\bar{e}}_1 = \bar{A}_{11}\, \bar{e}_1 + \bar{A}_{12}\, e_y - f_{3o} - G_3\, e_y\,, \qquad \dot{e}_y = A_{21o}\, \bar{e}_1 + \bar{A}_{22}\, e_y - f_{2o} - G_2\, e_y - v\,, \tag{6.28}$$

where the following new quantities are defined:

$$\bar{A}_{11} = A_{11o} + L\, A_{21o} \qquad \bar{A}_{12} = A_{12o} + L\, A_{22o} - A_{11o}\, L - L\, A_{21o} L\,, \quad \bar{A}_{22} = A_{22o} - A_{21o} L\,,$$

$$f_{3o} = f_{1o} + L\, f_{2o}\,, \qquad G_3 = G_1 + L G_2\,. \tag{6.29}$$

Let's assume the following:

$$G_3 = \bar{A}_{12}\,, \qquad G_2 = \bar{A}_{22} - A_{22}^{s}\,. \tag{6.30}$$

This gives

$$\dot{\bar{e}}_1 = \bar{A}_{11}\, \bar{e}_1 - f_{3o}\,, \qquad \dot{e}_y = A_{21o}\, \bar{e}_1 + A_{22}^{s}\, e_y - f_{2o} - v\,. \tag{6.31}$$

Let's consider a Lyapunov function V, defined as

$$V(t) = \boldsymbol{e}(t)^T \boldsymbol{P}\, \boldsymbol{e}(t), \tag{6.32}$$

where $\boldsymbol{e}(t) = \begin{Bmatrix} \bar{\boldsymbol{e}}_1 \\ \boldsymbol{e}_y \end{Bmatrix}$ and $\boldsymbol{P}$ is a symmetric positive definite matrix defined as

$$\boldsymbol{P} = \begin{bmatrix} \boldsymbol{P}_1 & 0 \\ 0 & \boldsymbol{P}_y \end{bmatrix}. \tag{6.33}$$

The symmetric positive definite matrices $\boldsymbol{P}_1$ and $\boldsymbol{P}_y$ are the solutions of the following Lyapunov equations:

$$\boldsymbol{P}_1 \bar{\boldsymbol{A}}_{11} + \bar{\boldsymbol{A}}_{11}^T \boldsymbol{P}_1 = -\boldsymbol{Q}_1, \qquad \boldsymbol{P}_y \boldsymbol{A}_{22}^s + \boldsymbol{A}_{22}^{s\,T} \boldsymbol{P}_y = -\boldsymbol{Q}_y, \tag{6.34}$$

where $\boldsymbol{Q}_1$ and $\boldsymbol{Q}_y$ are symmetric positive definite design matrices. After the matrix multiplication, Eq. (6.32) can be rewritten as

$$V(t) = \bar{\boldsymbol{e}}_1^T \boldsymbol{P}_1 \bar{\boldsymbol{e}}_1 + \boldsymbol{e}_y^T \boldsymbol{P}_y \boldsymbol{e}_y. \tag{6.35}$$

The time derivative of the Lyapunov function is

$$\dot{\boldsymbol{V}}(t) = 2\bar{\boldsymbol{e}}_1^T \boldsymbol{P}_1 (\bar{\boldsymbol{A}}_{11}\bar{\boldsymbol{e}}_1 - \boldsymbol{f}_{3o}) + 2\bar{\boldsymbol{e}}_y^T \boldsymbol{P}_y (\boldsymbol{A}_{21o}\bar{\boldsymbol{e}}_1 + \boldsymbol{A}_{22}^s \bar{\boldsymbol{e}}_y - \boldsymbol{f}_{2o} - \boldsymbol{v}). \tag{6.36}$$

In obtaining Eq. (6.36), we used the fact that the transpose of a scalar remains the same and substituted the time derivatives of the errors from Eqs. (6.31). Recognizing that the matrices $\boldsymbol{P}_1$ and $\boldsymbol{P}_y$ are symmetric and using Eqs. (6.34), we get

$$\dot{V}(t) = -\bar{\boldsymbol{e}}_{\boldsymbol{1}}{}^{T}\boldsymbol{Q}_{\boldsymbol{1}}\bar{\boldsymbol{e}}_{\boldsymbol{1}} - \boldsymbol{e}_{\boldsymbol{y}}{}^{T}\boldsymbol{Q}_{\boldsymbol{y}}\boldsymbol{e}_{\boldsymbol{y}} - 2\bar{\boldsymbol{e}}_{\boldsymbol{1}}{}^{T}\boldsymbol{P}_{\boldsymbol{1}}\boldsymbol{f}_{\boldsymbol{3o}} + 2\boldsymbol{e}_{\boldsymbol{y}}{}^{T}\boldsymbol{P}_{\boldsymbol{y}}\boldsymbol{A}_{\boldsymbol{21o}}\bar{\boldsymbol{e}}_{\boldsymbol{1}} - 2\,\boldsymbol{e}_{\boldsymbol{y}}{}^{T}\boldsymbol{P}_{\boldsymbol{y}}\,\boldsymbol{f}_{\boldsymbol{2o}} - 2\boldsymbol{e}_{\boldsymbol{y}}{}^{T}\boldsymbol{P}_{\boldsymbol{y}}\boldsymbol{v}\,. \quad (6.37)$$

Since the first two terms of the above equation are always positive, the following inequality holds

$$\dot{V}(t) \le -2\bar{\boldsymbol{e}}_{\boldsymbol{1}}{}^{T}\boldsymbol{P}_{\boldsymbol{1}}\boldsymbol{f}_{\boldsymbol{3o}} + 2\boldsymbol{e}_{\boldsymbol{y}}{}^{T}\boldsymbol{P}_{\boldsymbol{y}}\boldsymbol{A}_{\boldsymbol{21o}}\bar{\boldsymbol{e}}_{\boldsymbol{1}} - 2\boldsymbol{e}_{\boldsymbol{y}}{}^{T}\boldsymbol{P}_{\boldsymbol{y}}\,\boldsymbol{f}_{\boldsymbol{2o}} - 2\boldsymbol{e}_{\boldsymbol{y}}{}^{T}\boldsymbol{P}_{\boldsymbol{y}}\boldsymbol{v}\,. \quad (6.38)$$

We choose $\boldsymbol{v}$ as given below:

$$\boldsymbol{v} = \begin{cases} \rho_o \dfrac{\boldsymbol{P}_{\boldsymbol{y}}{}^{T}\boldsymbol{e}_{\boldsymbol{y}}}{\left\|\boldsymbol{P}_{\boldsymbol{y}}{}^{T}\boldsymbol{e}_{\boldsymbol{y}}\right\|} & \text{where } \left\|\boldsymbol{P}_{\boldsymbol{y}}{}^{T}\boldsymbol{e}_{\boldsymbol{y}}\right\| \neq \boldsymbol{0}, \\ \boldsymbol{0} & \text{otherwise.} \end{cases} \quad (6.39)$$

where ρ_o is a scalar design quantity. Substituting $\boldsymbol{v}$ from Eq. (6.39) into Eq. (6.38) gives

$$\dot{V}(t) \le -2\bar{\boldsymbol{e}}_{\boldsymbol{1}}{}^{T}\boldsymbol{P}_{\boldsymbol{1}}\boldsymbol{f}_{\boldsymbol{3o}} + 2\boldsymbol{e}_{\boldsymbol{y}}{}^{T}\boldsymbol{P}_{\boldsymbol{y}}\,\boldsymbol{A}_{\boldsymbol{21o}}\,\bar{\boldsymbol{e}}_{\boldsymbol{1}} - 2\boldsymbol{e}_{\boldsymbol{y}}{}^{T}\boldsymbol{P}_{\boldsymbol{y}}\,\boldsymbol{f}_{\boldsymbol{2o}} - 2\rho_o\frac{\boldsymbol{e}_{\boldsymbol{y}}{}^{T}\boldsymbol{P}_{\boldsymbol{y}}\boldsymbol{P}_{\boldsymbol{y}}{}^{T}\boldsymbol{e}_{\boldsymbol{y}}}{\left\|\boldsymbol{P}_{\boldsymbol{y}}{}^{T}\boldsymbol{e}_{\boldsymbol{y}}\right\|}\,. \quad (6.40)$$

The numerator of the last term in the above equation is basically the square of the denominator. This leads to

$$\dot{V}(t) \le -2\bar{\boldsymbol{e}}_{\boldsymbol{1}}{}^{T}\boldsymbol{P}_{\boldsymbol{1}}\boldsymbol{f}_{\boldsymbol{3o}} + 2\boldsymbol{e}_{\boldsymbol{y}}{}^{T}\boldsymbol{P}_{\boldsymbol{y}}\,\boldsymbol{A}_{\boldsymbol{21o}}\bar{\boldsymbol{e}}_{\boldsymbol{1}} - 2\boldsymbol{e}_{\boldsymbol{y}}{}^{T}\boldsymbol{P}_{\boldsymbol{y}}\,\boldsymbol{f}_{\boldsymbol{2o}} - 2\rho_o\left\|\boldsymbol{P}_{\boldsymbol{y}}{}^{T}\boldsymbol{e}_{\boldsymbol{y}}\right\|. \quad (6.41)$$

We can replace the first three terms by their magnitude and still the inequality will hold:

$$\dot{V}(t) \le 2\left\|\bar{\boldsymbol{e}}_{\boldsymbol{1}}{}^{T}\boldsymbol{P}_{\boldsymbol{1}}\boldsymbol{f}_{\boldsymbol{3o}}\right\| + 2\left\|\boldsymbol{e}_{\boldsymbol{y}}{}^{T}\boldsymbol{P}_{\boldsymbol{y}}\,\boldsymbol{A}_{\boldsymbol{21o}}\bar{\boldsymbol{e}}_{\boldsymbol{1}}\right\| + 2\left\|\boldsymbol{e}_{\boldsymbol{y}}{}^{T}\boldsymbol{P}_{\boldsymbol{y}}\,\boldsymbol{f}_{\boldsymbol{2o}}\right\| - 2\rho_o\left\|\boldsymbol{P}_{\boldsymbol{y}}{}^{T}\boldsymbol{e}_{\boldsymbol{y}}\right\|. \quad (6.42)$$

Using the Cauchy-Schwarz inequality (i.e., $\|\langle \boldsymbol{x}, \boldsymbol{y} \rangle\| \le \|\boldsymbol{x}\|\|\boldsymbol{y}\|$) and recognizing that the transpose of a scalar does not change the value, one can write

$$\dot{V}(t) \le 2 \left\| \boldsymbol{P_y}^T \boldsymbol{e_y} \right\| \left(\sqrt{\frac{\bar{\boldsymbol{e}}_{\boldsymbol{1}}^T \boldsymbol{P_1} \boldsymbol{P_1}^T \bar{\boldsymbol{e}}_{\boldsymbol{1}}}{\boldsymbol{e_y}^T \boldsymbol{P_y} \boldsymbol{P_y}^T \boldsymbol{e_y}}} \|\boldsymbol{f_{3o}}\| + \|\boldsymbol{A_{21o}} \bar{\boldsymbol{e}}_{\boldsymbol{1}}\| + \|\boldsymbol{f_{2o}}\| - \rho_o \right). \tag{6.43}$$

Now we use the Rayleigh principle, stated below:

$$\lambda_{\min}(\boldsymbol{Q}) \|\boldsymbol{x}\|^2 \le \boldsymbol{x}^T \boldsymbol{Q}\, \boldsymbol{x} \le \lambda_{\max}(\boldsymbol{Q}) \|\boldsymbol{x}\|^2 . \tag{6.45}$$

where $\lambda_{\min}$ and $\lambda_{\max}$ are the minimum and the maximum eigenvalues of $\boldsymbol{Q}$. Using the Rayleigh principle, Eq. (6.43) can be written as

$$\dot{V}(t) \le 2 \left\| \boldsymbol{P_y}^T \boldsymbol{e_y} \right\| \left(\sqrt{\frac{\lambda_{\max}(\boldsymbol{P_1} \boldsymbol{P_1}^T)}{\lambda_{\min}(\boldsymbol{P_y} \boldsymbol{P_y}^T)}} \frac{\|\bar{\boldsymbol{e}}_{\boldsymbol{1}}\|}{\|\boldsymbol{e_y}\|} \|\boldsymbol{f_{3o}}\| + \|\boldsymbol{A_{21o}} \bar{\boldsymbol{e}}_{\boldsymbol{1}}\| + \|\boldsymbol{f_{2o}}\| - \rho_o \right). \tag{6.46}$$

Equation (6.46) implies that $\dot{V}(t) \le 0$ as long as the following inequality holds:

$$\rho_o \ge \sqrt{\frac{\lambda_{\max}(\boldsymbol{P_1} \boldsymbol{P_1}^T)}{\lambda_{\min}(\boldsymbol{P_y} \boldsymbol{P_y}^T)}} \frac{\|\bar{\boldsymbol{e}}_{\boldsymbol{1}}\|}{\|\boldsymbol{e_y}\|} \|\boldsymbol{f_{3o}}\| + \|\boldsymbol{A_{21o}} \bar{\boldsymbol{e}}_{\boldsymbol{1}}\| + \|\boldsymbol{f_{2o}}\| . \tag{6.47}$$

This concludes the derivation of the sliding mode observer. The design parameters ρ_c and ρ_o for the controller and observer depend upon the uncertainty in the plant model and the magnitude of the external disturbances. A higher uncertainty and disturbance will lead to a higher design value of ρ_c and ρ_o. The trade-off is that higher magnitudes of these parameters will generally lead to high control voltages too. In the next section, we apply the sliding mode controller and observer for the vibration control problem.

6.5 Vibration Control

For a distributed structure, an exact representation of displacement or velocity in terms of modal coordinates would need an infinite number of modes. This implies that vibration control of a distributed structure in modal space would also require an infinite number of terms, which is impractical to consider. We generally ignore higher modes because, 1) the higher modes are difficult to excite and gives minimal contributions to the vibration, 2) higher modes are more prone to inaccuracies due to simplifications/assumptions in analysis, and 3) the frequency of excitation may be low enough so that the higher modes do not get excited. All the modes of the structure can be divided into three groups: 1) controlled modes, 2) modeled uncontrolled modes (residual modes), and 3) unmodeled modes, which are altogether ignored (Meirovitch, 1990). These three types of modes are usually arranged in an increasing order of frequency. The control voltages, which are calculated using the modal displacements and velocities of the controlled modes, also interact with the residual modes and unmodeled modes. This unwanted excitation of the remaining modes due to the limited number of discrete actuators causes the control spillover. Though the control spillover deteriorates the performance of a system, it is unlikely to cause any serious problem, such as instability. Similarly, the sensor outputs, which are used in estimating states using the observer, are affected by the residual and unmodeled modes. Apart from degrading the performance, the observation spillover can lead to instability (Balas, 1978). We will pay special attention to the observation spillover problem. Mathematical details of the above discussions can be found in Meirovitch (1990).

Next, we present the vibration control results where only the controlled modes are considered. After that, we include the residual modes and show the control and observation spillover effects. In order to improve the controller performance, we use both the controlled and residual modes in the observer. This reduces the observation spillover. Finally, we present the effects of parameter uncertainty and external disturbances on the performance of the controller. In all the cases, we will be using sliding mode control and sliding mode observer and the optimally designed actuators and sensors presented in Chapter 5.

6.5.1 Control Without Considering the Residual Modes

Figure 6.1 shows the initial condition response of the inflated torus considering the first nine modes. The residual modes are not considered. The states after the application of controller are also shown in Fig. 6.1. It can be seen from the figure that the settling time reduces by more than 4 sec. Also, there is a small decrease in the peak response. Figure 6.2 translates the states to the deflections at the five sensor locations. Similar reductions in the settling times and peak response can be observed there too. Figure 6.3 presents the state error (difference between the estimated states of the observer and the actual states). The error is initially high and goes to almost zero after around 0.25 sec. The actuator voltages were limited to 2 kV (Azzouz et al., 2001). The maximum applied voltage could be traded off with the performance of the controller.

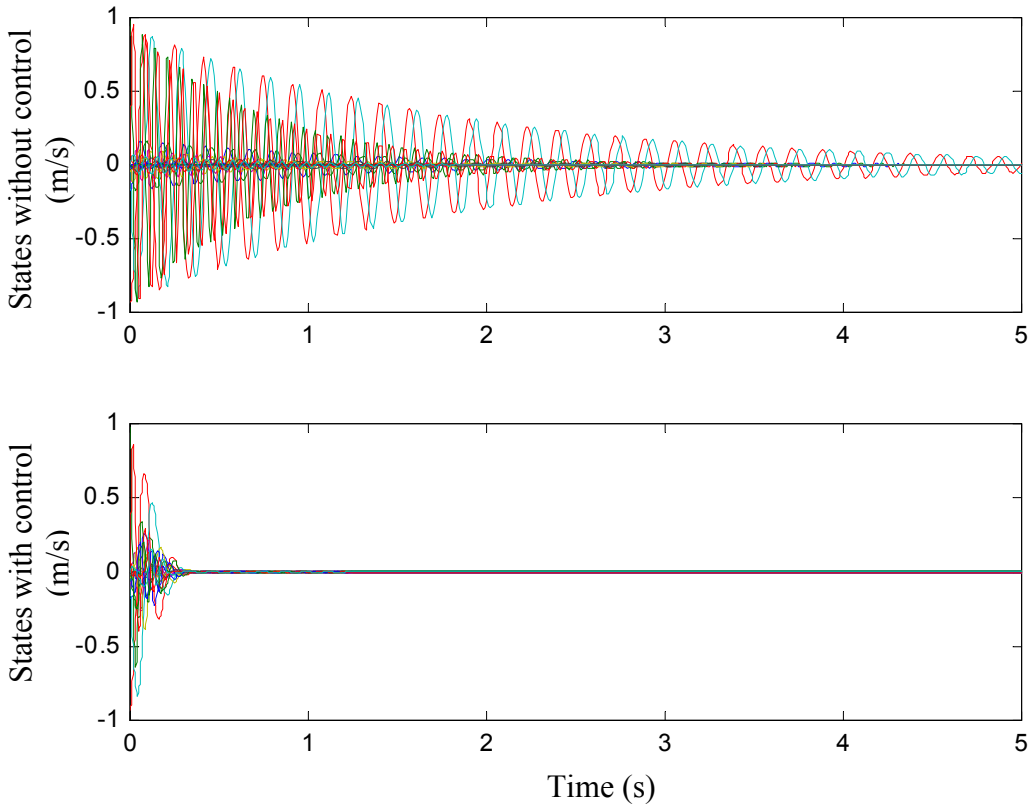

Fig. 6.1: Effect of controller on states without considering the residual modes.

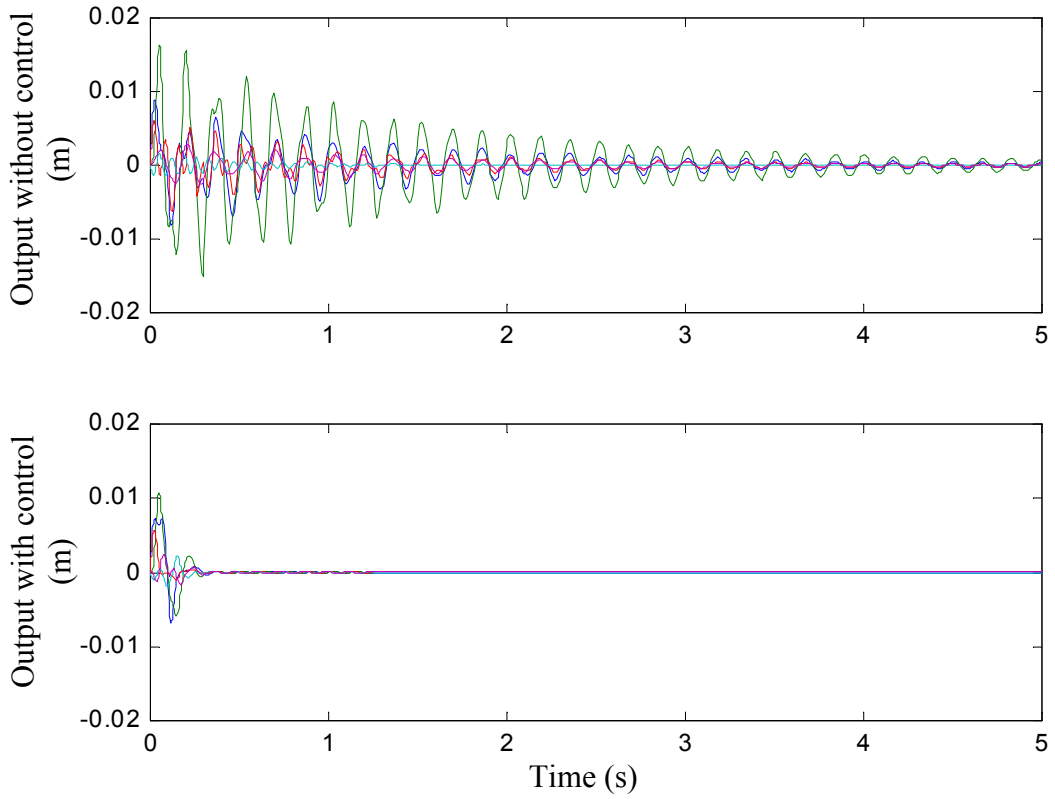

Fig. 6.2: Effect of controller on deflections without considering the residual modes.

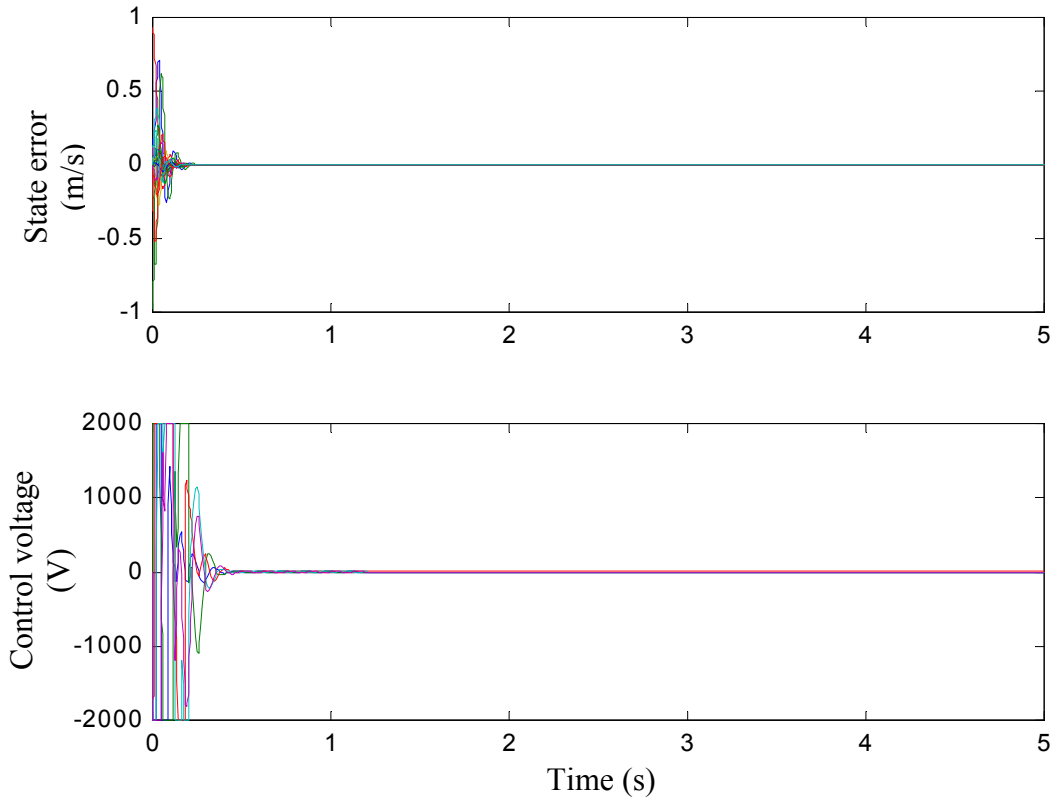

Fig. 6.3: State errors and control voltages without considering the residual modes.

6.5.2 Effects of Residual Modes

In Chapter 4, we saw that the frequencies of the inflated torus are quite close to each other. Therefore, the modes immediately above the controlled mode could very well contribute to the vibration of the torus. Taking into account the next five modes, we show the effects of the residual modes. As can be seen from state vs. time plots (Fig. 6.4), the controller is unable to suppress the vibration. For this reason, the deflection does not subside over time (Fig. 6.5). It was found that the main reason for such a dismal performance of the controller is the erroneous state estimation. Figure 6.6 illustrates the high state error, meaning that the observer fails to replicate the states. This gives rise to persistent actuator voltages of the maximum amplitude, which, in turn, produces persistent vibration. In the next subsection, we attempt to deal with this problem.

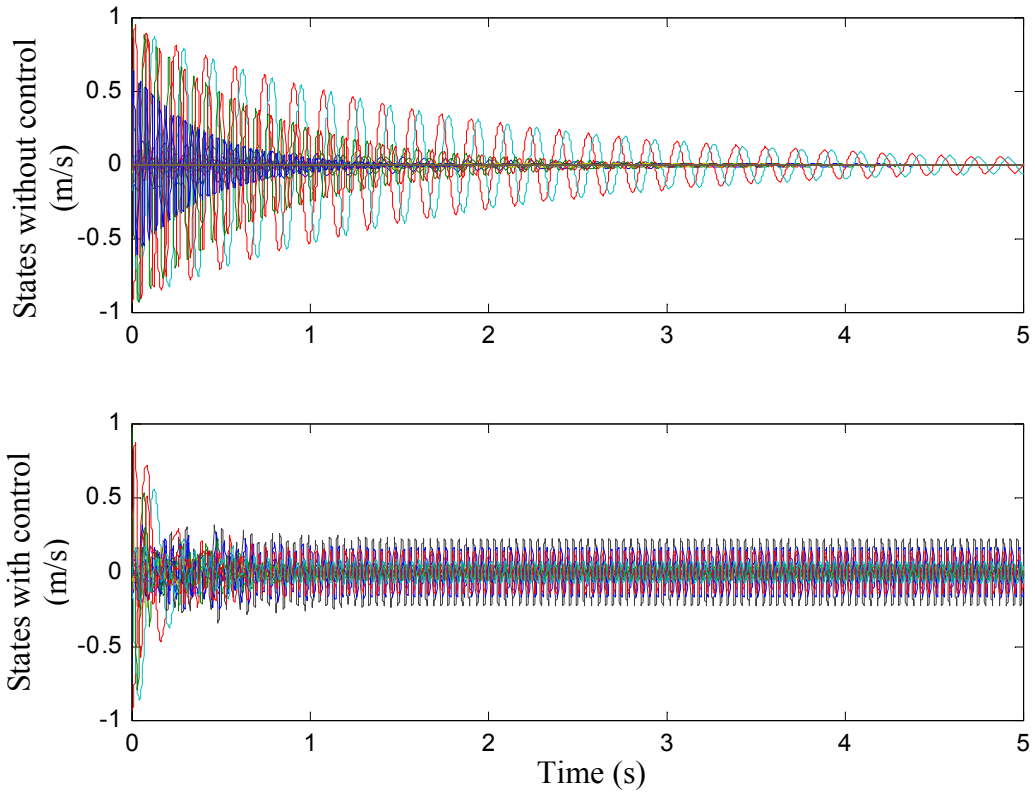

Fig. 6.4: Control and observation spillover effects on states.

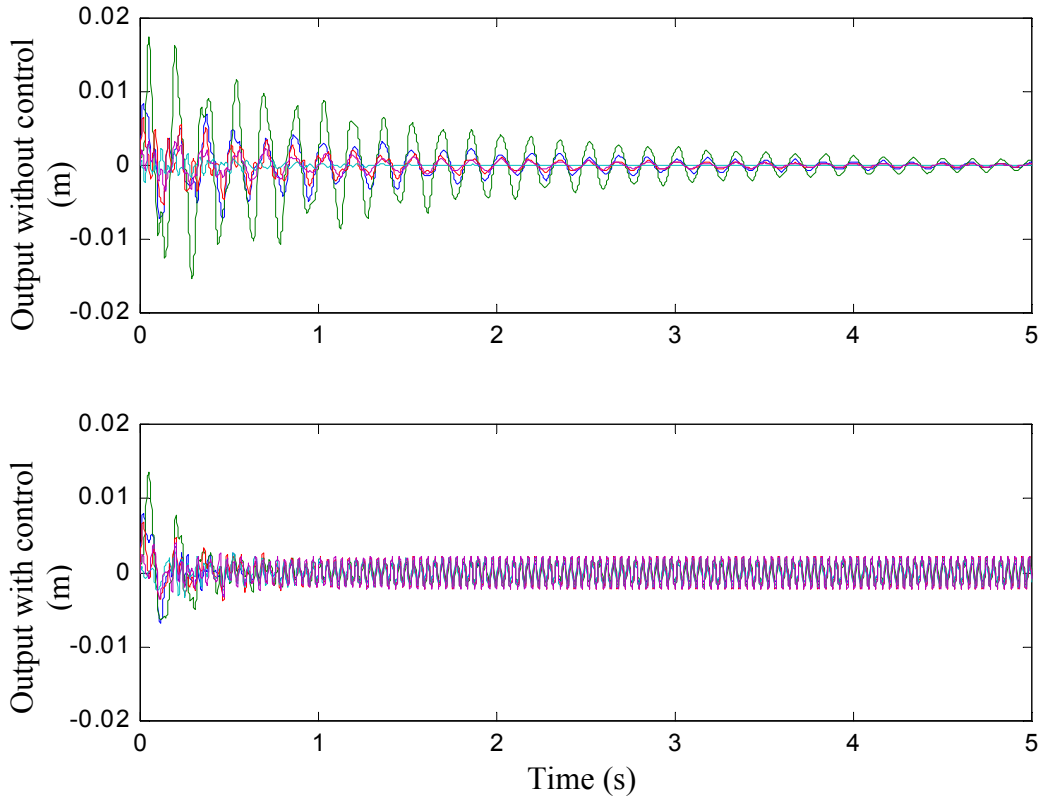

Fig. 6.5: Control and observation spillover effects on deflections.

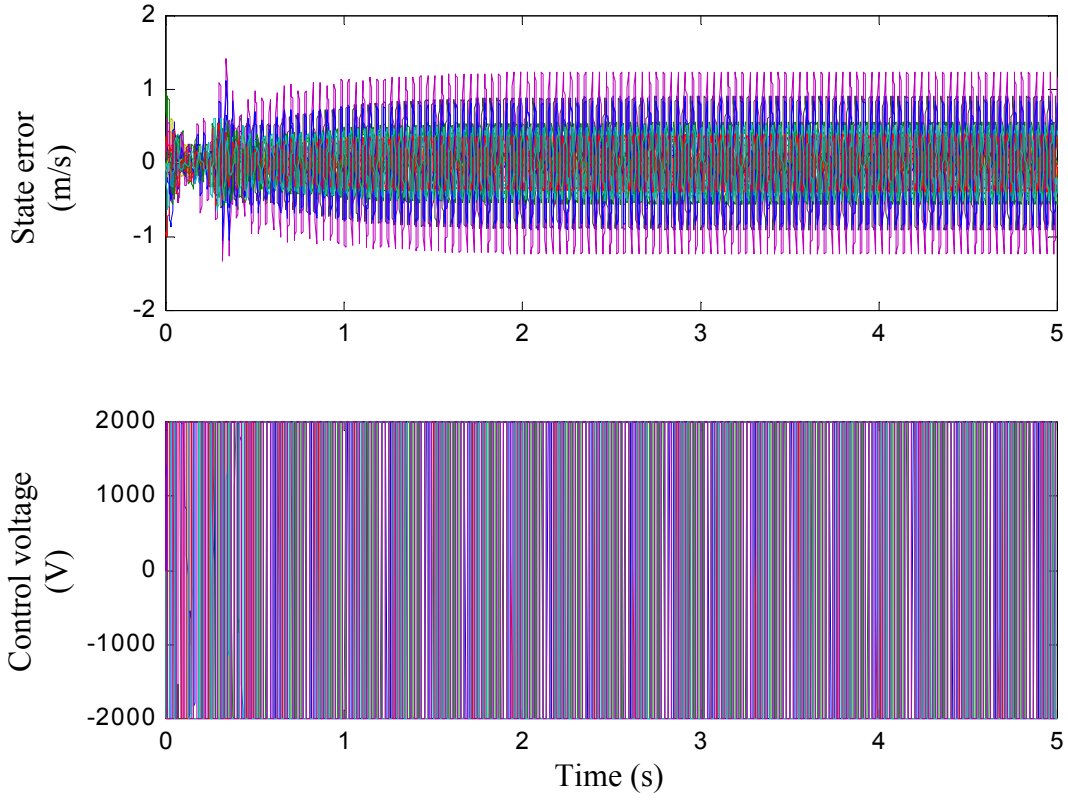

Fig. 6.6: Control and observation spillover effects on state errors and control voltages.

6.5.3 Reduction of Observation Spillover

Control and spillover effects worsen the performance of a controller. It was seen that the observation spillover effect is more critical since it makes the observer unable to estimate the states correctly. Several techniques are available to alleviate the observation spillover problem (Meirovitch and Baruh, 1983). For example, modal filtering could be used to obtain the modal displacements and velocities from the sensor measurement. This method, however, needs a large number of sensors so that the sensor data could be interpolated to find output at every point on the structure. Obviously, for a structure like a torus, one would need an unmanageable number of sensors. Another method is to include the residual modes in the observer. In this case, while the attempt is made to control the controlled modes, the observer is used in estimating the residual mode states as well. This minimizes the observation spillover and improves the performance of the controller as is evident from Figs. 6.7, 6.8, and 6.9. It can be noticed that the performance of the controller is far better than the case when the residual modes were not considered in the observer. However, the performance does degrade compared to the case of no residual effect.

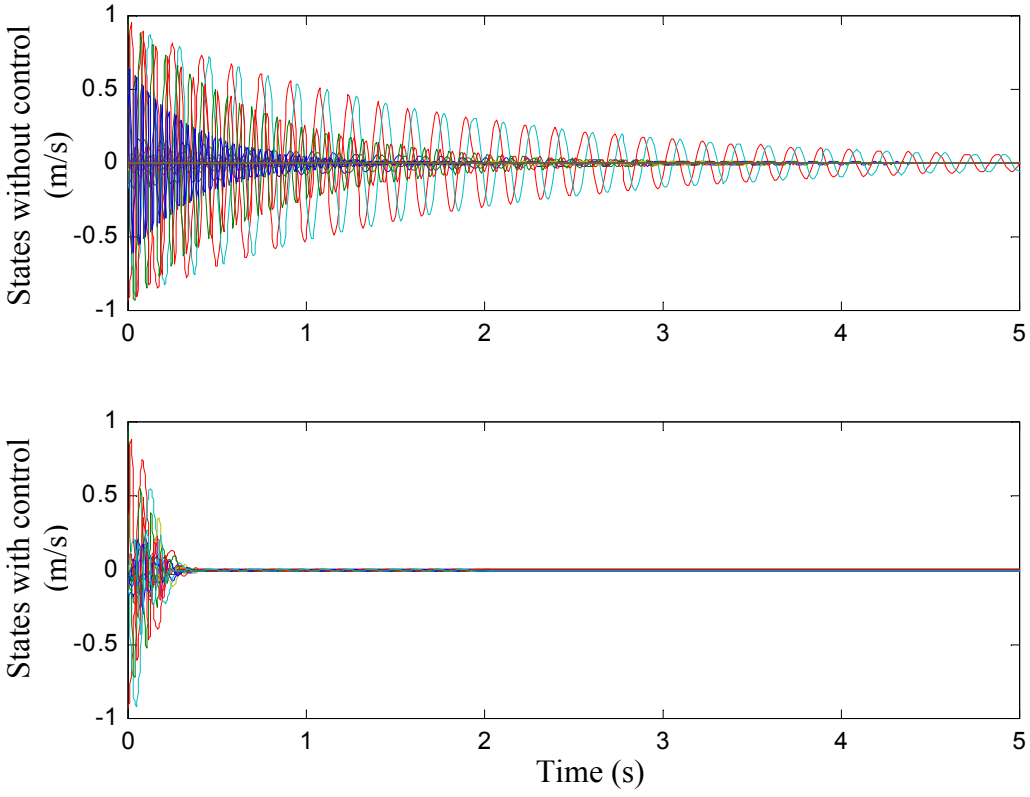

Fig. 6.7: Effect of controller on states after reducing the observation spillover.

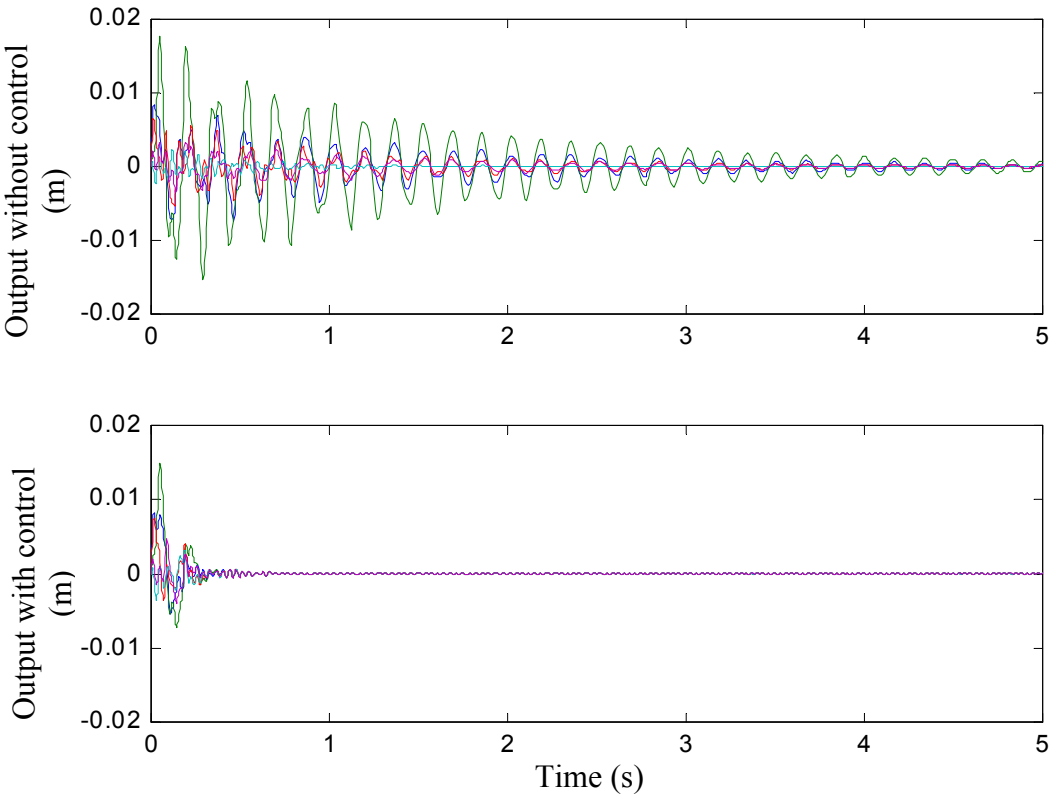

Fig. 6.8: Effect of controller on deflections after reducing the observation spillover.

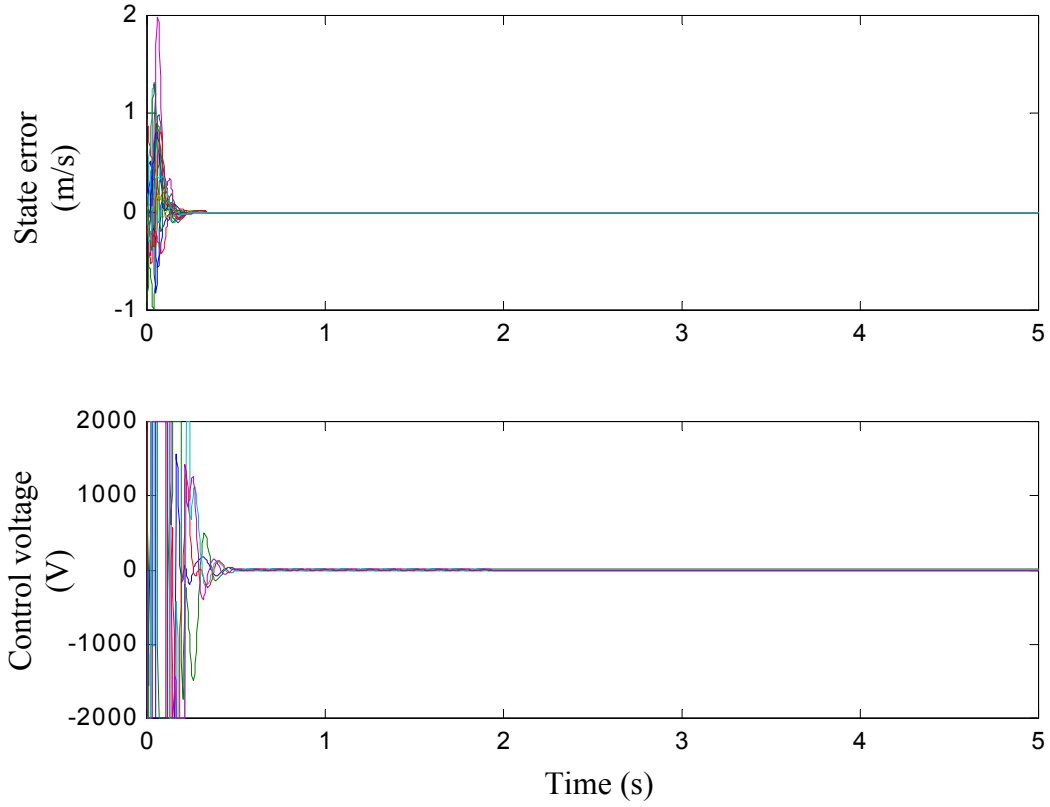

Fig. 6.9: State errors and control voltages after reducing the observation spillover.

6.5.4 Robustness of the Controller

It was mentioned earlier that the inflatable torus, being a part of the satellite antenna, could face varying temperature due to the varying amount of sunlight it faces as it goes from orbital day to orbital night. One of the important effects of the temperature change is to alter the internal pressure of the inflated torus. Since the major source of strength in an inflated structure is its internal pressure, it is worth evaluating the performance of the controller when the internal pressure is different from the design case. We consider here cases of 0.25 psi and 0.75 psi internal pressure. Note that the design internal pressure is 0.5 psi. Natural frequencies are shown in Table 6.1. The mode shapes are also affected due to the change in internal pressure (Fig. 4.9).

Table 6.1: Natural frequencies at different pressures including the passive effects.

Mode Number	Wave number, symmetry	Frequencies at 0.25 psi (Hz)	Frequencies at 0.5 psi (Hz)	Frequencies at 0.75 psi (Hz)
1	2, Symmetric	5.51	6.06	6.33
2	2, Symmetric	5.51	6.06	6.33
3	2, Antisymmetric	7.59	8.24	8.48
4	2, Antisymmetric	7.59	8.24	8.48
5	3, Symmetric	13.88	14.42	14.77
6	3, Symmetric	13.88	14.42	14.77
7	3, Antisymmetric	13.02	14.73	15.40
8	3, Antisymmetric	13.02	14.73	15.40
9	0, Antisymmetric	16.56	18.45	19.21
10	1, Antisymmetric	23.38	25.36	26.07
11	1, Antisymmetric	23.38	25.36	26.07
12	0, Symmetric	26.15	27.37	27.80
13	4, Antisymmetric	26.48	31.61	33.35
14	4, Antisymmetric	26.48	31.61	33.35

Due to changes in the natural frequencies and the mode shapes, the state-space model of the plant changes. However, the controller, which was designed using the nominal internal pressure (0.5 psi) is not updated. As in the previous section, we consider the spillover effects and design the observer for both controlled and residual modes. Figure 6.10 shows the effect of the controller on the states of the inflated torus at 0.25 psi. It can be noticed that the states die out as the time unfolds. Similarly, the deflection of the torus reduces with time (Fig. 6.11). The controller performs well for the internal pressure of 0.75 psi (Fig. 6.12). Comparing the two cases, one can conclude that at the higher pressure, the controller performance is better. Compared to the nominal case, we see that the performance is degraded in both cases. Note that this uncertainty changes all the matrices in the state-space model and hence it is not a matched uncertainty, which was used in the derivations of the sliding mode controller and observer. Next, we show how the controller performs in the presence of disturbances.

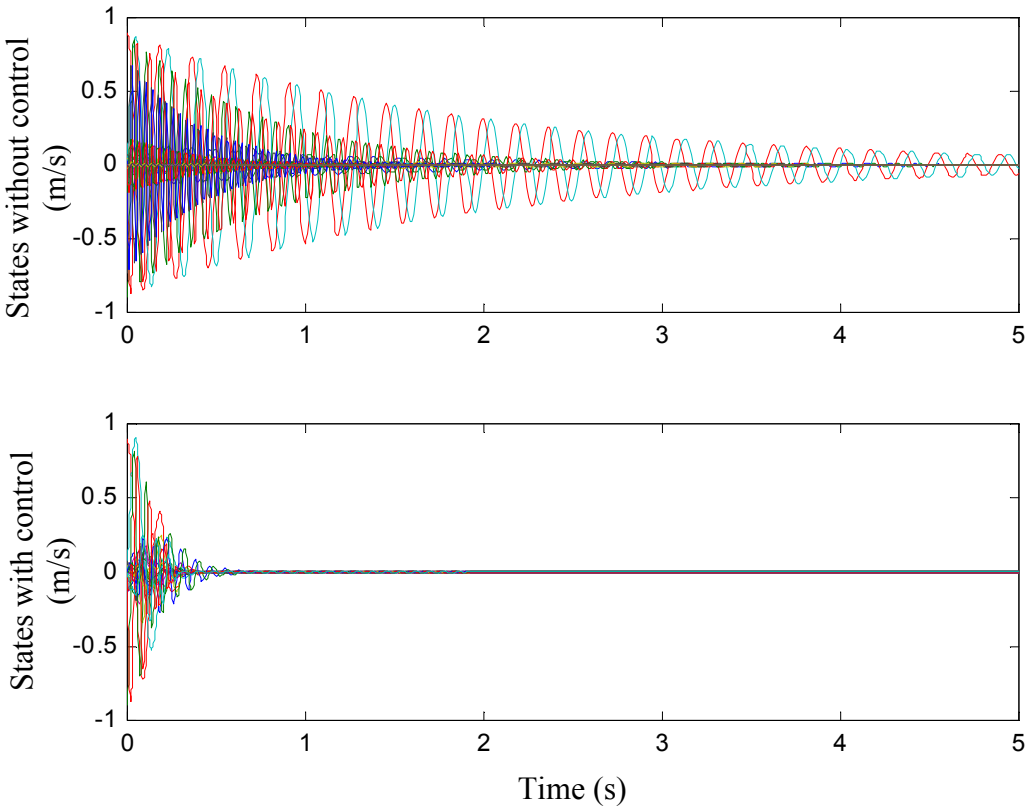

Fig. 6.10: Effect of controller on states at an internal pressure of 0.25 psi.

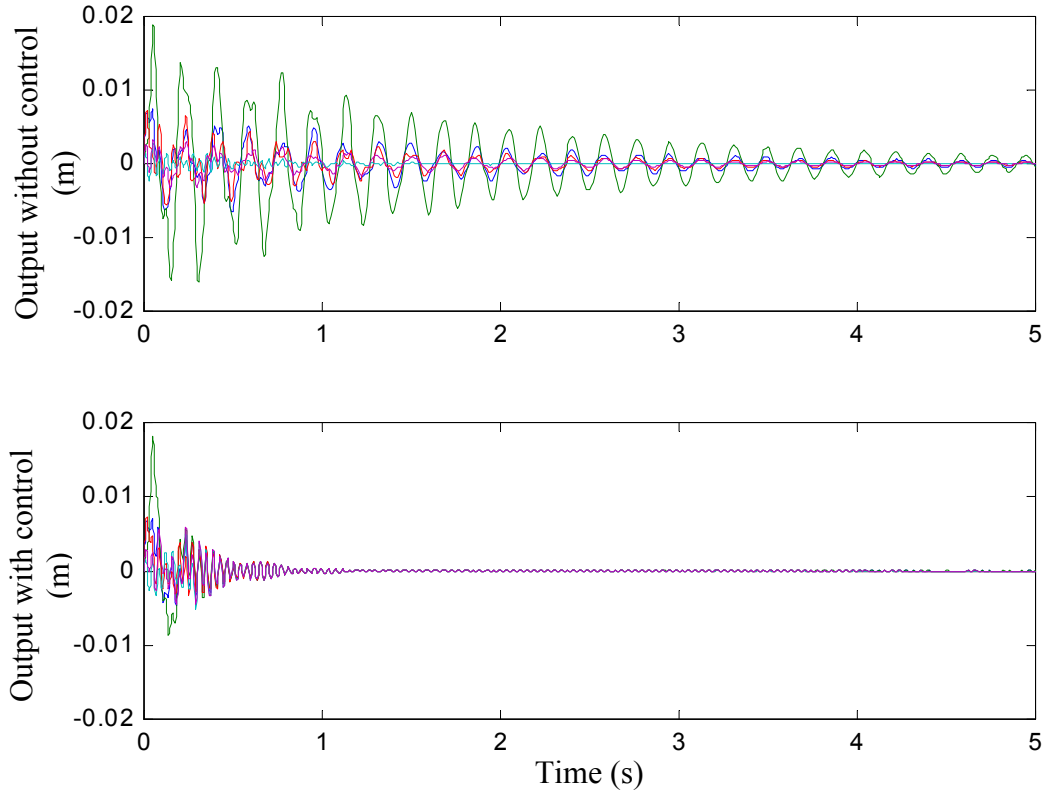

Fig. 6.11: Effect of controller on deflection at an internal pressure of 0.25 psi.

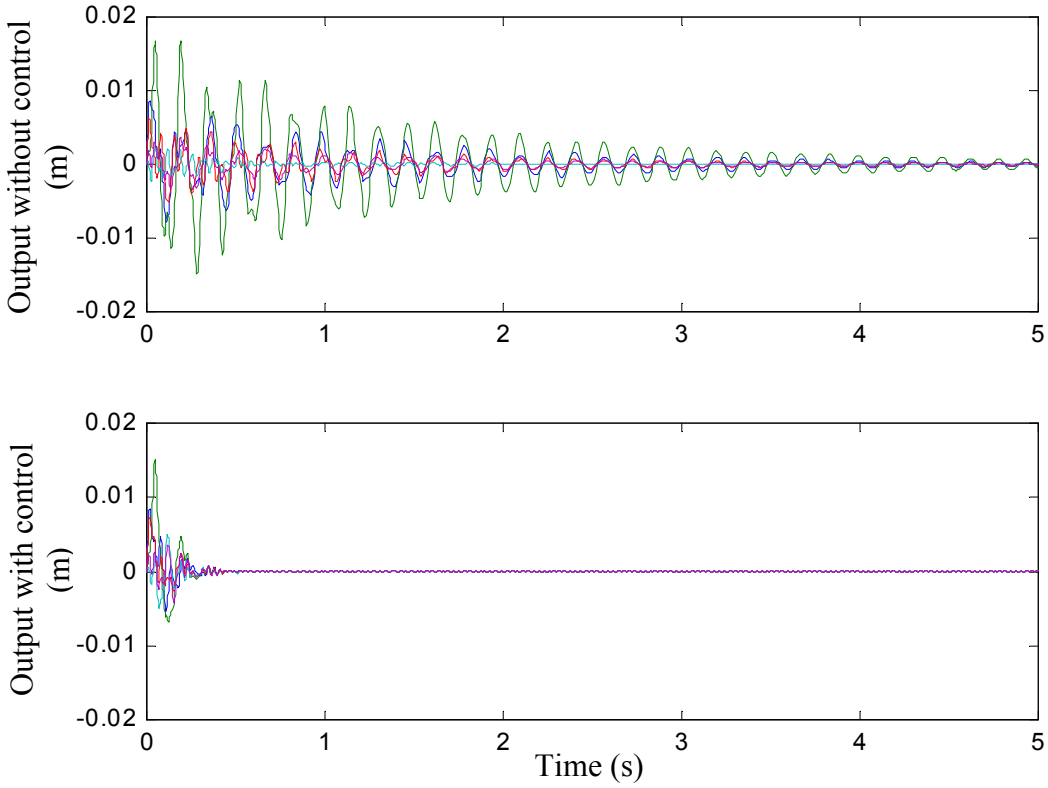

Fig. 6.12: Effect of controller on deflections at an internal pressure of 0.75 psi.

For the disturbance, we use a chirp signal. The frequency of the disturbance signal keeps increasing with time. The disturbances are assumed to interact with the system through the input channel, i.e., they are matched disturbances. Figure 6.13 shows the influence of disturbances on the deflection before and after the control action has been applied. Vibration reduction is evident from the figure. It can also be seen that the response of the system becomes less at a higher time (above 4.5 s). This is because, at higher time, the frequencies of the disturbance excitations become quite high compared to the frequencies of the controlled and residual modes. After around 4.5 s, we see that the uncontrolled and controlled response have similar magnitudes. It is due to the fact that, at higher time, the frequencies of the disturbance signals lie beyond the frequency bandwidth of the controller. It should be noted that the same controller has been used for all the cases presented in this chapter. This implies that the sliding mode observer and controller have successfully cancelled the uncertainty and disturbances within the frequency range of the controller.

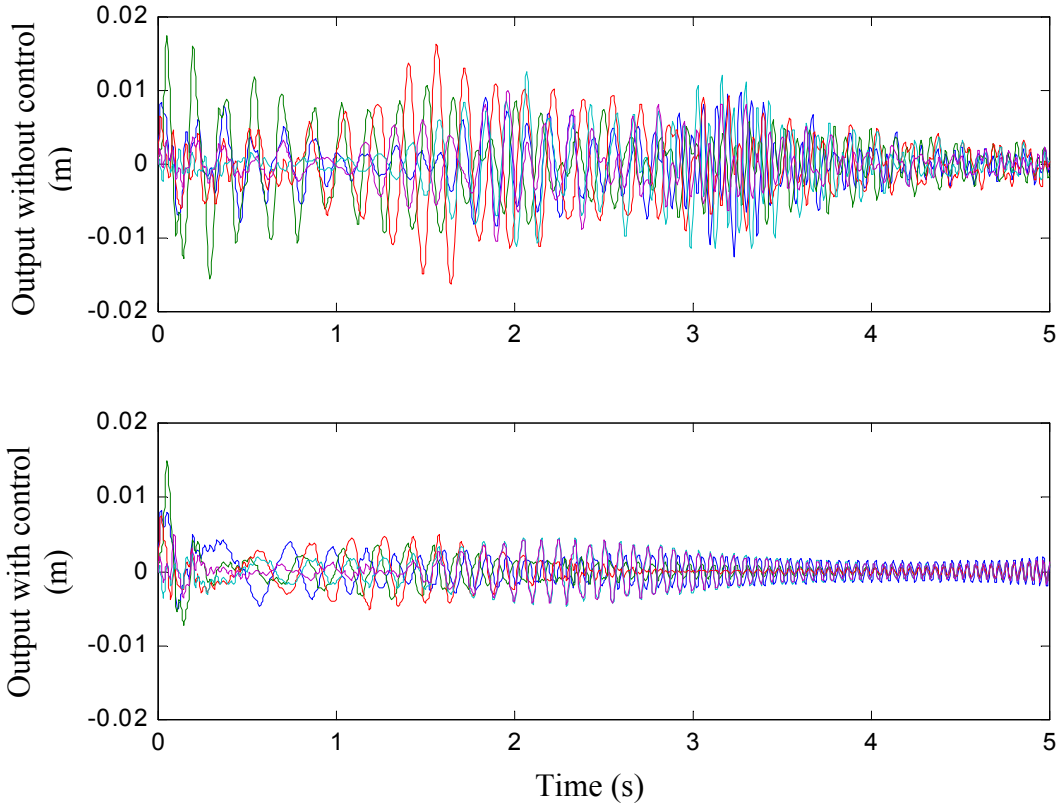

Fig. 6.13: Effect of controller on deflections subjected to external disturbances.

6.6 Conclusions

In this chapter, we presented vibration control analyses of an inflated torus. In order to achieve good vibration reduction performances under model uncertainty and external disturbances, a sliding mode controller and observer were used. The basics of the design approach were presented. Thereafter, we applied the methodology to control the initial condition response of the inflated torus considering the first nine modes. First, the controller was evaluated without considering the residual modes. The performance was found to be good. After that, we showed the control and observation spillover effects. As expected, the controller was unable to reduce the vibration. It was found that the observation spillover effect is more critical and is the main cause of the poor performance of the controller. In order to reduce the effect of observation spillover, the observer was designed considering the residual modes. The performance improved significantly. As described earlier, sliding mode controller and observer were chosen so as to counter the model uncertainty and disturbances. We examined the controller action for two different internal pressures, one above the nominal pressure and the other below. In both cases, the performance was adequate. It was seen that vibration reduction is better in the case of higher pressure. We also considered external matched disturbances and found good disturbance cancellation properties of the sliding mode controller and observer within the frequency bandwidth of the control system. As expected, we saw that as the characteristics of the structure change from their nominal values, the vibration reduction performance of the controller decreases.

From the above analysis, one can conclude that piezoelectric actuators and sensors could successfully be employed for the vibration reduction of an inflated torus. Compared to other simpler structures like beams and plates, we find that the vibration control of an inflated torus is more complicated. The primary reason for this behavior is the repeated or closely spaced natural frequencies and relatively complicated mode shapes.